AGU PUBLICATIONS

Paleoceanography

RESEARCH ARTICLE
10.1002/2015PA002840

Key Points:
- Our results provide the longest (1.2 Myr), most detailed record of North Pacific Intermediate Water
- Enhanced NPIW recurred during extreme glacials, when flow through the Bering Strait was cut off
- Our results challenge the idea of an NPIW-NADW seesaw proposed by some modelers

Supporting Information:
- Text S1, Figures S1–S3, and Tables S1–S6

Correspondence to:
K. P. Knudson and A. C. Ravelo,
kknudson@ucsc.edu;
acr@ucsc.edu

Citation:
Knudson, K. P., and A. C. Ravelo (2015), North Pacific Intermediate Water circulation enhanced by the closure of the Bering Strait, *Paleoceanography*, *30*, 1287–1304, doi:10.1002/2015PA002840.

Received 7 JUN 2015
Accepted 19 SEP 2015
Accepted article online 25 SEP 2015
Published online 21 OCT 2015
Corrected 4 DEC 2015

This article was corrected on 4 DEC 2015. See the end of the full text for details.

North Pacific Intermediate Water circulation enhanced by the closure of the Bering Strait

Karla P. Knudson[1] and Ana Christina Ravelo[2]

[1]Department of Earth and Planetary Sciences, University of California, Santa Cruz, California, USA, [2]Department of Ocean Sciences, University of California, Santa Cruz, California, USA

Abstract The Bering Strait provides a shallow connection that allows freshwater to flow from the North Pacific into the North Atlantic, but this passage was closed during past glacials when sea level was at least 50 m lower than at present. Climate models investigating Bering Strait closure predict that this mechanism increases the salinity in the North Atlantic and reduces the salinity in the North Pacific, inducing a Pacific-Atlantic seesaw in meridional overturning circulation and poleward heat flux. However, the Pacific circulation response to Bering Strait closure, and thus the seesaw theory, has not been tested by long paleoceanographic records. We present long records of foraminiferal $\delta^{18}O$ and $\delta^{13}C$ from Integrated Ocean Drilling Program Site U1342 in the Bering Sea, which provide the first evidence of enhanced North Pacific Intermediate Water when the Bering Strait was closed during each of the extreme glacials of the last 1.2 Myr. These results suggest that orbital-scale variations in North Pacific Intermediate Water are coherent and in phase with variations in upper North Atlantic Deep Water but are unrelated to changes in lower North Atlantic Deep Water. Together, these results provide evidence for systematic, orbital-scale variability in North Pacific Ocean circulation and may challenge the idea of an orbital-scale Pacific-Atlantic seesaw.

1. Introduction

The Bering Strait plays a central role in global climate by acting as a freshwater on-off switch modifying the centers of Northern Hemisphere deep water formation that participate in global meridional overturning circulation (MOC) [*Hu et al.*, 2012a, 2010, 2012b; *Saenko et al.*, 2004; *Shaffer and Bendtsen*, 1994]. Today, ~1 Sverdrup of the relatively low salinity North Pacific water that enters the Bering Sea flows through the Bering Strait into the Arctic Ocean before eventually feeding into the more saline North Atlantic [*Woodgate et al.*, 2012]. However, because the Bering Strait sill depth is extremely shallow (50 m), throughflow is highly vulnerable to sea level and thus global climate. During extreme glacials, such as the Last Glacial Maximum (LGM; ~20 ka), the closure of the Bering Strait isolated the North Pacific from the North Atlantic, which is thought to have had profound implications for deep/intermediate water formation and climate feedbacks in both major ocean basins [*Hu et al.*, 2015, 2012a, 2010, 2012b; *Okazaki et al.*, 2010; *Saenko et al.*, 2004; *Shaffer and Bendtsen*, 1994].

Many model simulations demonstrate that a strong salinity gradient between the Atlantic and Pacific drives opposed changes, or a *seesaw*, in subsurface circulation strength between the two basins [e.g., *Hu et al.*, 2015, 2012a, 2010; *Okazaki et al.*, 2010; *Saenko et al.*, 2004]. Models looking at the effect of Bering Strait closure predict that isolating the Atlantic from the Pacific causes saltier North Atlantic surface water, decreased stratification, and enhanced Atlantic MOC (AMOC), while simultaneously causing fresher North Pacific surface waters and weaker Pacific MOC (PMOC) [*Hu et al.*, 2015, 2010]. Consequently, these models predicting seesaw behavior indicate that a closed Bering Strait makes the North Atlantic/North Pacific relatively warm/cool compared to an open strait scenario, and this seesaw behavior is superimposed on, and exists independently from, background conditions [*Hu et al.*, 2015, 2010].

In order to test the seesaw hypothesis maintained by modeling results, we need to assess long geological records of the major water masses associated with Northern Hemisphere MOC: North Atlantic Deep Water (NADW) and North Pacific Intermediate Water (NPIW). However, so far, the length and quality of records from the North Pacific have been inadequate for determining recurring trends, and available short records do not provide a clear picture of whether or not there was systematic seesaw behavior during the last glacial periods. Observational records investigating millennial-scale seesaw behavior have been limited to the last ~30 kyr and are contradictory, with some radiocarbon evidence supporting the presence of seesaw behavior during

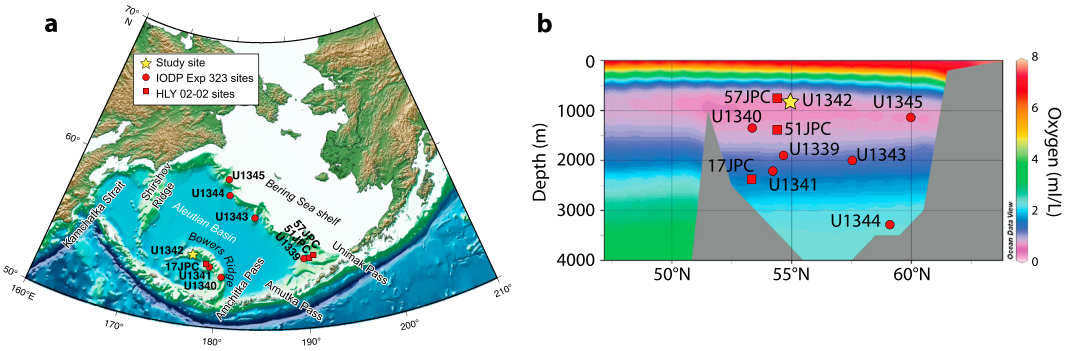

Figure 1. Bering Sea site maps. (a) Locations of IODP Expedition 323 sites in the Bering Sea are marked with red circles (Site U1342 starred), and HLY-02-02 sites are marked with red squares. (b) Bering Sea vertical dissolved oxygen profile along the 180° transect. Site U1342 is located just below the depth of modern NPIW, making it ideal for detecting an enhanced and expanded NPIW water mass. Modified from *Expedition 323 Scientists* [2010].

Heinrich Event 1 and the Younger Dryas [*Max et al.*, 2014; *Okazaki et al.*, 2010] and other radiocarbon [*Sarnthein et al.*, 2013] and temperature [*Max et al.*, 2012] evidence supporting in-phase relationships between the Atlantic and Pacific. No records have yet investigated possible orbital-scale seesaw behavior. Moreover, records shorter than one glacial-interglacial (G/IG) cycle cannot determine long-term circulation trends in the context of major climate transitions nor distinguish how deep and intermediate water masses may differ between weak and strong glacials. Given the importance of understanding how connections through the world's oceans affect regional and global climate, our study aims to use long paleoceanographic records to assess the NPIW-NADW relationship on G/IG timescales. Here we use new, long cores from Integrated Ocean Drilling Program (IODP) Expedition 323 (Figure 1a) in the Bering Sea to generate the first records of orbital-scale changes in NPIW spanning many G/IG cycles over the last 1.2 Myr. These records are then used in comparison with existing orbital-scale records of NADW to reveal observational evidence contradicting the seesaw hypothesis proposed by modeling studies.

2. North Pacific Intermediate Water and the Bering Sea

NPIW, the densest water mass formed in the modern North Pacific Ocean [*Talley*, 2003], is formed when surface water sinks, carrying atmospherically equilibrated oxygen into the ocean's interior in a process known as "ventilation." Today, NPIW mostly forms within the Sea of Okhotsk during wintertime sea ice formation, when expelled brine produces extremely dense water masses [*Shcherbina et al.*, 2003; *Yasuda*, 1997]. The most active regions of brine production occur on the continental shelf within coastal polynyas—open water surrounded by sea ice [*Shcherbina et al.*, 2003; *Schumacher et al.*, 1983].

Evidence for enhanced North Pacific ventilation at shallow to middepths during the LGM [*Cook et al.*, 2005; *Horikawa et al.*, 2010; *Matsumoto et al.*, 2002; *Okazaki et al.*, 2005; *Tanaka and Takahashi*, 2005] has led to the theory that Northern Hemisphere glacial climates are associated with increased NPIW production. The Bering Sea, which has deep connections to the Pacific and was strongly ventilated during the last glacial, has been a suggested source of NPIW [*Horikawa et al.*, 2010; *Ohkushi et al.*, 2003; *Rella et al.*, 2012; *Tanaka and Takahashi*, 2005]. Trace amounts of deep water recently formed within the Bering Sea demonstrate its potential to supply significant NPIW during glacial periods when sea ice formation and brine rejection were enhanced [*Warner and Roden*, 1995], and high salinities (up to 35 practical salinity units (psu)) within Bering Sea polynyas support the feasibility of this mechanism.

3. Study Area

The Bering Sea exchanges water with the North Pacific through the Kamchatka Strait (~4000 m sill depth) and the Near Strait (~2000 m sill depth), which remain open during both glacials and interglacials, allowing the Bering Sea to continuously record changes in North Pacific intermediate and deep water conditions. The focus of our study is the shallowest IODP Expedition 323 site, U1342 (Figure 1a; 818 m water depth), which is ideally situated for detecting changes in NPIW, as it is located near the present-day oxygen minimum zone

(~1000 m; Figure 1b) and the ventilation depth during the last glacial [Horikawa et al., 2010]. Due to its location on the top of Bowers Ridge, Site U1342 also likely benefits from winnowing, which removes organic matter and contributes to excellent foraminifera preservation. The sedimentation rate (4.5 cm/kyr) at this site is high enough to resolve orbital-scale variability but lower compared to other Expedition 323 Bering Sea sites (up to 45 cm/kyr) and other Bowers Ridge sites (12 cm/kyr), allowing longer exposure time of the sediment to the deep water. As a consequence, profiles of interstitial water sulfate, dissolved inorganic carbon, phosphate, and ammonium demonstrate that this site has low rates of anaerobic carbon mineralization [*Expedition 323 Scientists*, 2011]. Compared to Site U1341 (Figure 1), a deeper site on the flank of Bowers Ridge with much higher sedimentation rates, U1342 displays ammonium concentrations an order of magnitude lower and phosphate concentrations 50% lower [*Expedition 323 Scientists*, 2011], further demonstrating the low mineralization rates that benefit Site U1342. Thus, even though the Bering Sea is a region of high productivity, Site U1342 has interstitial chemistry that is less altered by aerobic and anaerobic respiration, and better foraminifera preservation, compared to all other sites drilled during Expedition 323 [*Expedition 323 Scientists*, 2011]. Due to these advantages, benthic foraminiferal stable carbon isotope measurements can be reliably employed to record water mass changes at Site U1342, as we will later discuss in more detail.

4. Materials and Methods

4.1. Benthic Foraminiferal $\delta^{13}C_c$ and $\delta^{18}O_c$

Cores from Site U1342 were sampled at ~1–3 cm intervals, and one to three tests (usually three) of the benthic foraminifera *Uvigerina peregrina* were picked from the >250 μm fraction, sonicated, and analyzed for calcite $\delta^{13}C$ and $\delta^{18}O$ ($\delta^{13}C_c$ and $\delta^{18}O_c$) at the University of California-Santa Cruz (UCSC) Stable Isotope Laboratory using a FISONS Prism mass spectrometer with a common acid bath device and a MAT253 mass spectrometer with an online Kiel device. Values are reported in the per mil (‰) notation relative to Vienna Peedee belemnite (VPDB). Reproducibility of in-house standards is 0.07‰ for $\delta^{18}O$ and 0.03‰ for $\delta^{13}C$. In addition, four to five individual *U. peregrina* tests from six different samples representing peak glacials were measured for $\delta^{13}C_c$ and $\delta^{18}O_c$.

4.2. Benthic Foraminiferal Mg/Ca

U. peregrina from three G/IG pairs were analyzed for Mg/Ca ratios. G/IG pairs were selected based on a rapid $\delta^{18}O_c$ transition, large difference in $\delta^{18}O_c$ G/IG values, and foraminifera availability. Prior to analysis, crushed samples were cleaned according to a modified "Boyle protocol" [*Boyle and Keigwin*, 1985; *Lea and Boyle*, 1993]: samples were rinsed and sonicated in Milli-Q and methanol, cleaned with reductive and oxidative agents, and transferred into 1.5 mL acid-cleaned vials for a weak acid leach and final Milli-Q rinse. Mg/Ca ratios were analyzed at UCSC using a Perkin-Elmer Optima 8300 inductively coupled plasma optical emission spectrometer. Long-term reproducibility for a liquid consistency standard and foraminifera standards are 0.0254 mmol/mol and 0.176 mmol/mol, respectively.

4.3. Carbonate-Free Sediment Stable Isotope Analyses

Sediments for carbonate-free analysis were freeze-dried and crushed by hand using a mortar and pestle, acidified using a buffered solution of glacial acetic acid, and rinsed and centrifuged several times to remove acid. Samples were analyzed for $\delta^{13}C$, wt % C, and C:N ratio on a Carlo Erba 1108 elemental analyzer interfaced to a Thermo Finnigan Delta Plus XP isotope ratio mass spectrometer, at the UCSC Stable Isotope Laboratory. Carbon mass accumulation rate (CMAR) was calculated as dry bulk density × sedimentation rate × wt % C.

4.4. Age Model and Spectral Analyses

The U1342 age model, Blackman-Tukey spectral analyses, and cross-phase spectra were completed with *AnalySeries* 2.0 [*Paillard et al.*, 1996]. The U1342 age model was created using tie points to the LR04 $\delta^{18}O_c$ stack from *Lisiecki and Raymo* [2005] (Figure 2a and supporting information Table S1), and therefore, these records can be compared relative to each other. A discussion of the use of the LR04 stack in tuning the U1342 age model can be found in the supporting information (Text S1).

4.5. Stable Isotope Difference Calculations

To compare $\delta^{13}C_c$ from Site U1342 to Ocean Drilling Program (ODP) Site 849 (0°11′N, 110°31′W; 3851 m) [Mix et al., 1995], U1342 $\delta^{13}C_c$ values have been converted to the $\delta^{13}C_c$ values of *Cibicidoides wuellerstorfi*, using

the standard adjustment of +0.90‰ demonstrated by other studies [*Duplessy et al.*, 1984; *Mix et al.*, 1995]. To better compare the records at Site U1342 and Site 849, slight adjustments were made to update the published Site 849 age model (see supporting information Table S2). $\Delta\delta^{13}C$ and $\Delta\delta^{18}O$ values were calculated based on absolute U1342 $\delta^{13}C_c$ and $\delta^{18}O_c$ values, which were interpolated to the average interval between U1342 samples (~1.4 kyr), averaged over a three-point running window, and then subtracted from a similarly interpolated record from Site 849. By using this method, high-frequency millennial-scale variability at U1342 was smoothed out, allowing for the comparison of orbital variations between the records at U1342 and lower-resolution records from other sites. To compare North Atlantic sites ODP Site 982 (57°31′N, 15°53′W; 1135 m) [*Venz et al.*, 1999] and Deep Sea Drilling Project (DSDP) Site 607 (41°00′N, 32°58′W; 3427 m) [*Ruddiman et al.*, 1989] to Site 849, $\Delta\delta^{13}C$ for both data sets was similarly calculated, using an interpolation interval of 1.5 kyr.

4.6. Glacial Versus Interglacial and Open Versus Closed Bering Strait

Where applicable, "glacial" or "interglacial" points were defined as those 1 sigma above or below a 100 kyr moving window of an interpolated three-point running mean of U1342 $\delta^{18}O_c$. Data were further classified according to whether relative sea level (RSL) was above and below −50 m (open versus closed Bering Strait). RSL from 0 to 514 ka was assigned from *Rohling et al*. [2009], and RSL from 515–1200 ka was assigned from *Sosdian and Rosenthal* [2009]. These RSL estimates are precise enough to capture the general orbital-scale relationship between RSL and water mass distribution, even though the magnitude of local variations in RSL in the Bering Strait region may differ by ~25% [e.g., *Clark et al.*, 2002] from the global RSL variations, depending on local isostatic adjustment and the individual effect of ice sheet volume changes, or "fingerprinting."

5. Stable Isotope Results From U1342

5.1. U1342 $\delta^{18}O$ Stratigraphy and Age Model

The new record of benthic $\delta^{18}O_c$ at Site U1342 was used to create the first published age model for this site (supporting information Table S1) and displays all marine isotope stages (MIS) since 1.2 Ma (Figure 2a). The values of $\delta^{18}O_c$ range from ~2.5 to ~4.5‰, with typical G/IG change of only ~1‰. Comparison with the LR04 benthic stack [*Lisiecki and Raymo*, 2005]—a compilation of 57 globally distributed $\delta^{18}O_c$ records used to represent the global average—indicates that the G/IG $\delta^{18}O_c$ range at U1342 (~1‰) is smaller than that of the LR04 stack (~1.5‰) primarily because the glacial (high $\delta^{18}O_c$) values at U1342 are not as extreme (Figure 2a). The relatively small G/IG $\delta^{18}O_c$ amplitude at U1342 appears robust, as the quality of the record is supported by high sedimentation rates, continuous recovery, and continuous foraminifera preservation. Additionally, single foraminifer replicates show little $\delta^{18}O_c$ variability ($1\sigma = 0.08$ to 0.20‰; supporting information Table S3), indicating that mixing (bioturbation) between G/IG extremes is not responsible for the relatively low-amplitude $\delta^{18}O_c$ variability.

5.2. U1342 $\delta^{13}C$ Stratigraphy

The $\delta^{13}C_c$ record at Site U1342 displays values ranging between about −1.5‰ and 0.7‰, with most of the lowest values occurring in the oldest 250 kyr of the record. Compared to two records that may be taken to represent whole-Pacific records of $\delta^{13}C$, the Lisiecki deep Pacific $\delta^{13}C_c$ Stack [*Lisiecki*, 2010] and the Site 849 $\delta^{13}C_c$ record from *Mix et al*. [1995], Site U1342 approximately matches these records during most glacials and has lower (more negative) values during most interglacials (Figure 2b).

6. Evidence for Bering Sea Brine Formation and Ventilation

6.1. Changes in $\delta^{18}O$ Indicate Bering Sea Brine

The finding that the U1342 $\delta^{18}O_c$ record generally displays such a small G/IG change compared to global and regional records is perplexing at first glance and merits explanation. In general, $\delta^{18}O_c$ reflects local water temperature and local $\delta^{18}O$ of seawater ($\delta^{18}O_{sw}$), which is related to global ice volume and also typically to local changes in precipitation and evaporation (and thus salinity). Notably, the G/IG $\delta^{18}O_c$ range at U1342 is roughly equivalent to the change (~1‰) attributed to global ice volume alone [*Sosdian and Rosenthal*, 2009]. However, given the changes in U1342 $\delta^{13}C_c$ discussed later, and suggestions from a short record of

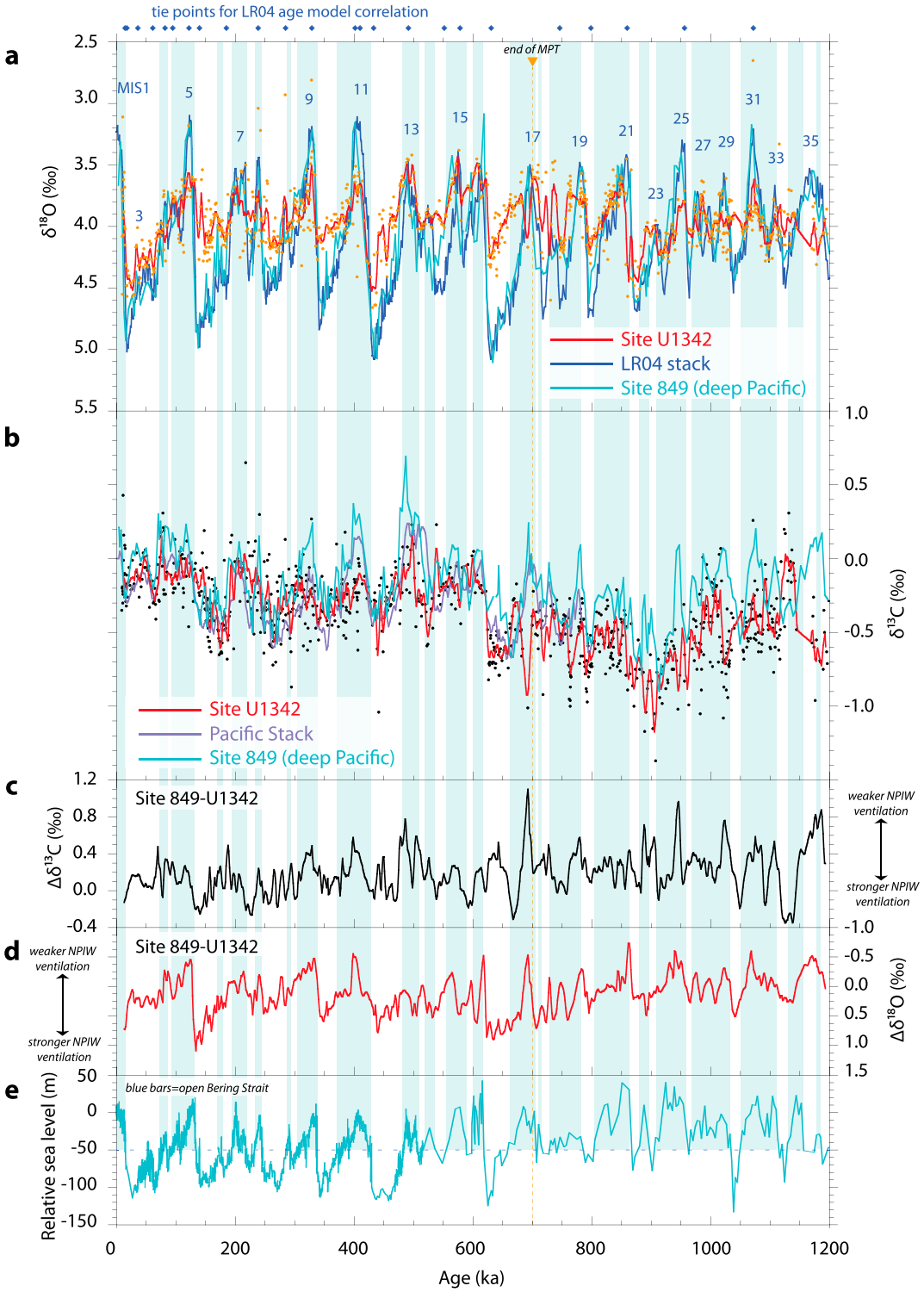

Figure 2. Geochemical records showing changes in climate and NPIW. (a) Benthic foraminiferal $\delta^{18}O_c$ records from Site U1342 (red line indicates three-point smoothed, interpolated running mean, and orange dots indicate original data points), the LR04 stack (dark blue line) from *Lisiecki and Raymo* [2005], and deep equatorial Pacific Site 849 (teal blue line) from *Mix et al.* [1995]. Blue diamonds show tie points used for U1342 age model age correlation with the LR04 stack. (b) Benthic foraminiferal $\delta^{13}C_c$ of Site U1342 (red line indicates three-point smoothed, interpolated running mean, and black dots indicate original data points), compared with Site 849 (teal blue line) and the deep Pacific stack from *Lisiecki* [2010] (blue line). (c) $\Delta\delta^{13}C_{849\text{-}U1342}$ is used here as a proxy for the presence of NPIW. (d) $\Delta\delta^{18}O_{849\text{-}U1342}$ is also an indicator of NPIW ventilation. (e) Relative sea level: 0–514 ka from *Rohling et al.* [2009] and 515–1200 ka from *Sosdian and Rosenthal* [2009]. Blue vertical bars correspond with values above the Bering Strait depth (dashed line; −50 m), indicating open Bering Strait conditions. The end of the Mid-Pleistocene Transition (MPT; 700 ka) is marked by the vertical dotted orange line.

Table 1. U1342 Average Benthic Foraminiferal $\delta^{18}O_c$ (‰) and Mg/Ca

	MIS	Average $\delta^{18}O_c$ (‰)	Average Mg/Ca
Interglacial	MIS 1	3.90	0.90
	MIS 5	3.68	0.82
	MIS 9	3.30	0.78
Glacial	MIS 2	4.50	0.79
	MIS 6	4.19	0.90
	MIS 10	4.09	0.73

neodymium isotopes at a nearby site [*Horikawa et al.*, 2010], it is unlikely that the character of the water bathing Site U1342 was constant throughout the past 1.2 Myr. We posit that the relatively low $\delta^{18}O_c$ amplitude of G/IG variations can be explained by a local water source formed by brine rejection during glacials. Brine rejection increases local salinity without significantly fractionating oxygen isotopes [*Brennan et al.*, 2013; *Hillaire-Marcel and de Vernal*, 2008; *Tan and Fraser*, 1976; *Tan and Strain*, 1996], creating a dense water mass capable of transmitting the extremely low-$\delta^{18}O_{sw}$ Bering Sea surface water to intermediate depths. Thus, the $\delta^{18}O_{sw}$ at U1342 would decrease if the water bathing this site changed from a Pacific source entering the Bering Sea from the south to include a stronger local Bering Sea surface water source. Local brine has been previously implicated to explain negative $\delta^{18}O_c$ excursions in deep North Pacific benthic records [*Gebhardt et al.*, 2008].

To test the idea that glacial brine formation within the Bering Sea resulted in a local low-$\delta^{18}O_{sw}$ glacial influence at U1342, we performed additional analyses in order to quantify G/IG changes in seawater temperature and $\delta^{18}O_{sw}$. In general, anomalously low $\delta^{18}O_c$ glacial values may theoretically be attributed to either bottom water warming or a water mass source with relatively low $\delta^{18}O_{sw}$ values (e.g., Bering Sea brine). To rule out warming as the explanation, we measured U1342 benthic foraminiferal Mg/Ca as a proxy of bottom water temperature and then quantitatively assessed G/IG changes in $\delta^{18}O_{sw}$, based on bottom water temperature measurements and global ice volume data. Mg/Ca results from three selected G/IG pairs are summarized in Tables 1 and 2, with all data shown in the supporting information Table S4. Considering the relationship between $\delta^{18}O_c$ and bottom water temperature (typically −0.23‰/+1°C) [*Ravelo and Hillaire-Marcel*, 2007], the three G/IG pairs in Table 2 would need to demonstrate ~2–3°C *warmer* temperature if local $\delta^{18}O_{sw}$ was *not* lower during the glacials (relative to the interglacials). However, based on the Mg/Ca temperature estimates, local $\delta^{18}O_{sw}$ calculations (Table 2) yield local $\Delta\delta^{18}O_{sw}$ difference values (glacial minus interglacial) that are negative in all three G/IG pairs. These $\delta^{18}O_{sw}$ calculations show that there was a local source of relatively low $\delta^{18}O_{sw}$ during each glacial, in agreement with the mechanism of local brine formation and ventilation.

Salinity changes due to changes in evaporation, precipitation, and runoff cannot explain the low glacial values of $\delta^{18}O_c$ at Site U1342. These processes result in a positive relationship between salinity and $\delta^{18}O_{sw}$ [*LeGrande and Schmidt*, 2006], and thus, the observed relatively low glacial $\delta^{18}O_{sw}$ at U1342, if related to these hydrological processes, would imply relatively *low* glacial salinity. However, it is implausible for lower salinity water to have occurred at the depth of Site U1342. In the modern ocean, North Pacific surface salinity is so low that surface waters are not dense enough to sink to appreciable depths, even when temperatures are near freezing [*Warren*, 1983]. An even lower salinity surface water mass would only create stronger stratification, prohibiting a low $\delta^{18}O_{sw}$ signal from reaching Site U1342.

To demonstrate this point, we use the observed $\Delta\delta^{18}O_{sw}$ (from Table 2) and the North Pacific relationship of $\Delta\delta^{18}O_{sw} = 0.44 \times SSS$ from *LeGrande and Schmidt* [2006], in which SSS is sea surface salinity (‰), to calculate the theoretical ΔSSS across all three IG/G terminations shown in Table 2. These calculations show ΔSSS

Table 2. Calculations of Glacial Minus Interglacial Bottom Water Temperature and $\delta^{18}O_{sw}$

Glacial − Interglacial	$\Delta\delta^{18}O_c$ (‰)	ΔMg/Ca	ΔBottom Water Temperature (°C)[a]	$\Delta\delta^{18}O_{sw}$ (‰)	$\Delta\delta^{18}O_{sw}$ Expected From Ice Volume (‰)[b]	Local $\Delta\delta^{18}O_{sw}$ (‰)
MIS 2 − 1	0.60	−0.11	−1.58	0.23	1.00	−0.77
MIS 6 − 5	0.51	0.07	1.03	0.75	1.06	−0.31
MIS 10 − 9	0.79	−0.05	−0.70	0.63	0.97	−0.34

[a]Bottom water temperature calculations based on measured Mg/Ca using the calibration from *Bryan and Marchitto* [2008]: $Mg/Ca = 0.86 + 0.071(T)$.
[b]$\delta^{18}O_{sw}$ change attributed to glacial ice volume: 0.1‰/−10 m of sea level. Sea level estimates from *Rohling et al.* [2009].

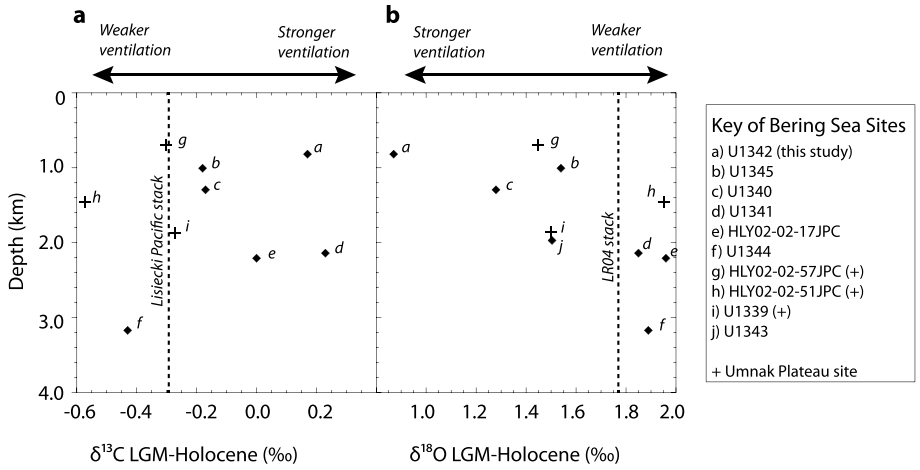

Figure 3. Comparison of ventilation influence on Bering Sea sites. (a) LGM $\delta^{13}C_c$ − Holocene $\delta^{13}C_c$ and (b) LGM $\delta^{18}O_c$ − Holocene $\delta^{18}O_c$ for sites HLY02-02-17JPC, HLY02-02-57JPC, and HLY02-02-51JPC; IODP Expedition 323 Sites U1342, U1345, U1340, U1341, U1343, U1344, and U1339. Data are from this study (U1342), *Asahi et al*. [2014] (U1343), and compiled by M. S. Cook et al. (Tracing Bering Sea circulation with benthic foraminiferal stable isotopes during the Pleistocene, submitted to *Deep Sea Research*) (all other sites). Sites g–i are from the Umnak Plateau, remotely located on the western margin of the Bering Sea, where circulation may have been limited (see Figure 1). LGM-Holocene isotopic differences from Bering Sea sites are compared to records of whole-ocean changes from the Lisiecki deep Pacific stack [*Lisiecki*, 2010] and the LR04 benthic stack [*Lisiecki and Raymo*, 2005] (dotted lines). The LGM was defined as Marine Isotope Stage 2 based on stratigraphy (maximum $\delta^{18}O_c$).

ranging from −0.70 to −1.75 psu. Although we argue later that models do not adequately represent brine formation, an important mechanism for NPIW formation, the models provide insight into the open sea convection process. Modeling results from *Hu et al*. [2012a] show that North Pacific surface water freshening of −0.70 to −1.75 psu would result in reduced open ocean convection, regardless of whether the Bering Strait is open or closed, and another model from *Menviel et al*. [2012] shows that deep North Pacific convection and deep/intermediate water formation can only arise by increasing surface water salinity. These results show that it would be impossible for surface water with relatively low glacial $\delta^{18}O_{sw}$ values to become dense enough to sink to the depth of Site U1342 if that water was of lower salinity. Thus, the relatively low glacial $\delta^{18}O_{sw}$ values must have had anomalously high salinity values, as this would be the only way to explain how water with such low $\delta^{18}O_{sw}$ values could have been dense enough to be recorded at the depth of U1342 during glacials. Therefore, brine rejection from sea ice formation, which can increase salinity and density of surface water without increasing $\delta^{18}O_{sw}$, very likely played an important role in NPIW ventilation in the past.

6.2. Bering Sea Regional Comparison

While there are no other Bering Sea records of $\delta^{18}O_c$ and $\delta^{13}C_c$ of similar length to compare to our stable isotope records from U1342, a regional comparison of shorter records reveals trends consistent with the idea of Bering Sea brine formation during the LGM. A compilation of shorter Bering Sea records (Figure 3 and supporting information Figure S1 and Table S5) shows that the amplitude of glacial $\delta^{18}O_c$ is dampened at intermediate depths (<2000 m) compared to deeper sites (>2000 m) and to the global average (represented by the LR04 stack). Strong glacial ventilation at intermediate depths (<2000 m), caused by a relatively high contribution of local Bering Sea surface water relative to deep Pacific-sourced water, is indicated by the relatively high $\delta^{13}C_c$ and low $\delta^{18}O_c$ values during the LGM compared to the Holocene. On the other hand, deep Bering Sea and North Pacific sites display isotopic changes similar to the Lisiecki deep Pacific stack [*Lisiecki*, 2010] and the LR04 benthic stack, [*Lisiecki and Raymo*, 2005] indicating little change in circulation in the deep (>2000 m) Pacific. This comparison, and evidence from the North Pacific during the last deglaciation [*Jaccard and Galbraith*, 2013], shows that intermediate depths were well ventilated from a surface water source, while the deep ocean was not.

Furthermore, $\delta^{18}O_c$ data from other oceans show that the Bering Sea had an unusual water structure profile during the LGM. The difference between $\delta^{18}O_c$ values in the LGM compared to the Holocene for Site U1342

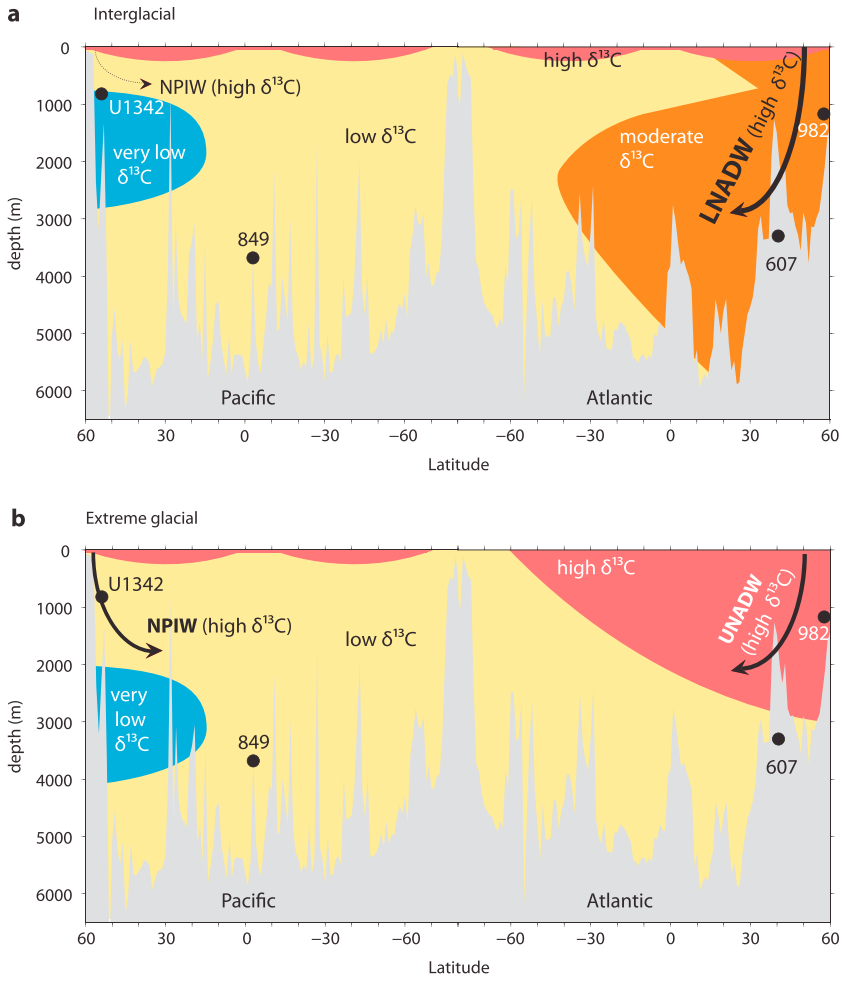

Figure 4. Schematic diagrams of the effect of ventilation on oceanic $\delta^{13}C$. (a) Interglacial scenario, showing that ventilation was relatively weak for both the Upper North Atlantic and North Pacific compared to (b) extreme glacial conditions, when both NPIW and UNADW formation were relatively strong. Generally, high $\delta^{13}C$ reflects relatively strong ventilation as surface waters sink into the intermediate and deep ocean. Since deep water is produced in the Atlantic but not in the Pacific, Atlantic Sites 982 and 607 typically have higher $\delta^{13}C$ compared to the Pacific Sites U1342 and 849. Using Site 849 to represent whole-ocean conditions, $\Delta\delta^{13}C_{849\text{-}U1342}$ can be used to measure relative changes NPIW ventilation, and $\Delta\delta^{13}C_{849\text{-}982}$ and $\Delta\delta^{13}C_{849\text{-}607}$ can be used to indicate the relative strength of UNADW and LNADW ventilation. Pacific and Atlantic bathymetry are along 171°W and 30°W longitude, respectively.

(0.87‰) is less than that of other oceans at intermediate depths, including the North Atlantic (~2‰) [*Keigwin*, 2004], the South Atlantic (~2‰) [*Curry and Oppo*, 2005], the South Pacific (~1.5‰) [*Herguera et al.*, 1992], and the Indian Ocean (1.1‰) [*Kallel et al.*, 1988]. Thus, the small LGM-Holocene $\delta^{18}O_c$ difference observed at Site U1342 is a unique feature for intermediate waters and is consistent with the idea of locally formed brine.

Assuming that variability in $\delta^{13}C_c$ and $\delta^{18}O_c$ can be used to examine changes in local ventilation, a compilation of Bering Sea $\delta^{13}C_c$ and $\delta^{18}O_c$ records would, hypothetically and ideally, delineate a regional isotopic water mass structure that reflects the influence of this ventilation. However, our method of looking at the *relative* changes (LMG-Holocene) in $\delta^{13}C_c$ and $\delta^{18}O_c$ at each site is currently the best method for assessing changes in brine formation during the last glacial, because there are not yet enough comparable data sets from various Bering Sea sites to be able to use *absolute* values to define regional isotopic water mass structure. Figure 3 and supporting information Table S5 provide a comprehensive list of the available $\delta^{13}C_c$ and $\delta^{18}O_c$ Bering Sea records. While there are records from 10 Bering Sea sites (including this study), records from seven of those sites cannot be directly compared to Site U1342 due to the use of a different foraminifera species (at 57JPC, U1341, 17JPC, and U1344), an unavailable $\delta^{13}C_c$ record (at U1343), and a remote site location not sensitive to circulation changes (at 51JPC and U1339). Using the three remaining sites (U1342, U1345, and

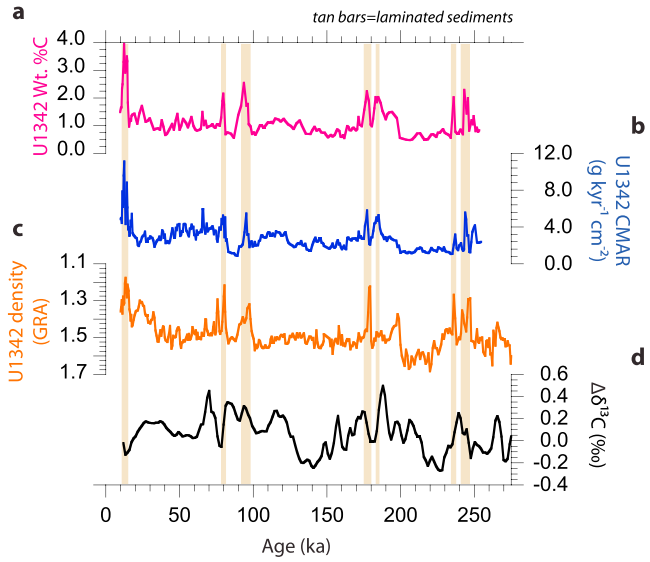

Figure 5. Multiple records of primary productivity are independent of the NPIW proxy $\Delta\delta^{13}C$. U1342 proxies of primary productivity, including (a) wt % C, (b) carbon mass accumulation rate (CMAR), and (c) sediment density measured by gamma ray attenuation (GRA) [*Expedition 323 Scientists*, 2011], show weak correlation compared to (d) the NPIW proxy of benthic foraminiferal $\Delta\delta^{13}C_{849\text{-}U1342}$. Tan vertical bars represent low-density laminated sediments representative of high productivity, which are also not well correlated to $\Delta\delta^{13}C$. This multiproxy comparison indicates that $\Delta\delta^{13}C$ is not dominated by fluctuations in organic carbon, justifying the use of $\Delta\delta^{13}C_{849\text{-}U1342}$ as an NPIW indicator.

U1340) to assess regional patterns in absolute $\delta^{13}C_c$ and $\delta^{18}O_c$ values is difficult, given their different locations within the basin (shelf versus ridge; Figure 1), possible variations in age models, and the fact that changes in productivity over time may affect the $\delta^{13}C_c$ at the other two sites more due to their much higher sedimentation rates (up to 30 cm/kyr). Therefore, as described above, using the data that is currently available, the best method for looking at changes in water mass conditions is to calculate relative differences in $\delta^{13}C_c$ and $\delta^{18}O_c$; this approach demonstrates enhancement in local Bering Sea ventilation during the LGM compared to the Holocene. Determining whether the LGM-like pattern of enhanced intermediate water ventilation (NPIW) is a robust and repeated feature of all glacial periods requires long records of $\delta^{13}C_c$ and $\delta^{18}O_c$ at U1342 over the last 1.2 Myr.

7. The Influence of North Pacific Intermediate Water in the Bering Sea

7.1. Proxies of NPIW: $\Delta\delta^{18}O$ and $\Delta\delta^{13}C$

In order to monitor changes in ventilation, inferred to be related to changes in the strength and/or characteristic of NPIW at Site U1342 over multiple G/IG timescales, it is necessary to have proxies that are unencumbered by the effects of whole-ocean chemical changes, which can occur on long timescales. Thus, rather than using absolute values of $\delta^{18}O_c$ and $\delta^{13}C_c$, we have determined two "new" proxies to resolve NPIW orbital-scale variability over the past 1.2 Myr. To subtract the influence of whole-ocean changes and isolate the regional influence of NPIW on the U1342 $\delta^{18}O_c$ and $\delta^{13}C_c$ records, we compare our records to Site 849 [*Mix et al.*, 1995], a deep Pacific site (0°11′N, 110°31′W; 3851 m) often used to represent global oceanic values. Thus, as proxies of the local influence of NPIW, we calculate $\Delta\delta^{18}O$ values (the $\delta^{18}O_c$ at Site 849 minus the $\delta^{18}O_c$ at U1342) and $\Delta\delta^{13}C$ values (the $\delta^{13}C_c$ at Site 849 minus the $\delta^{13}C_c$ at U1342), rather than using the absolute $\delta^{18}O_c$ and $\delta^{13}C_c$ values from U1342.

Due to temperature and salinity differences, $\delta^{18}O_c$ values at U1342 are presently lower than at Site 849. With enhanced NPIW ventilation, low-$\delta^{18}O_{sw}$ Bering Sea surface waters reaching Site U1342 would further decrease the $\delta^{18}O_c$ recorded here, resulting in higher $\Delta\delta^{18}O$ values. Thus, we interpret relatively high/low $\Delta\delta^{18}O$ values to indicate enhanced/reduced NPIW influence at U1342.

At any given location, the $\delta^{13}C$ of foraminiferal calcite ($\delta^{13}C_c$) reflects the $\delta^{13}C$ of dissolved inorganic carbon ($\delta^{13}C_{DIC}$) in seawater at that site, which is influenced by whole-ocean chemistry, the local balance between photosynthesis and respiration, and local relative mixtures of water masses with distinct $\delta^{13}C_{DIC}$ signatures [*Ravelo and Hillaire-Marcel*, 2007]. Deep, aged water masses accumulate the respiration products of exported marine organic matter and thus have low $\delta^{13}C_{DIC}$ values, while carbon uptake imparts higher $\delta^{13}C_{DIC}$ values on surface waters. In the modern ocean, deep Pacific water flows northward toward the Bering Sea, progressively aging and acquiring a lower $\delta^{13}C_{DIC}$ signature, and $\Delta\delta^{13}C$ is a relatively large value that reflects this aging process (Figure 4a). However, in an enhanced NPIW scenario, Site U1342 is strongly influenced by a relatively high $\delta^{13}C_{DIC}$ signature from its proximal surface water

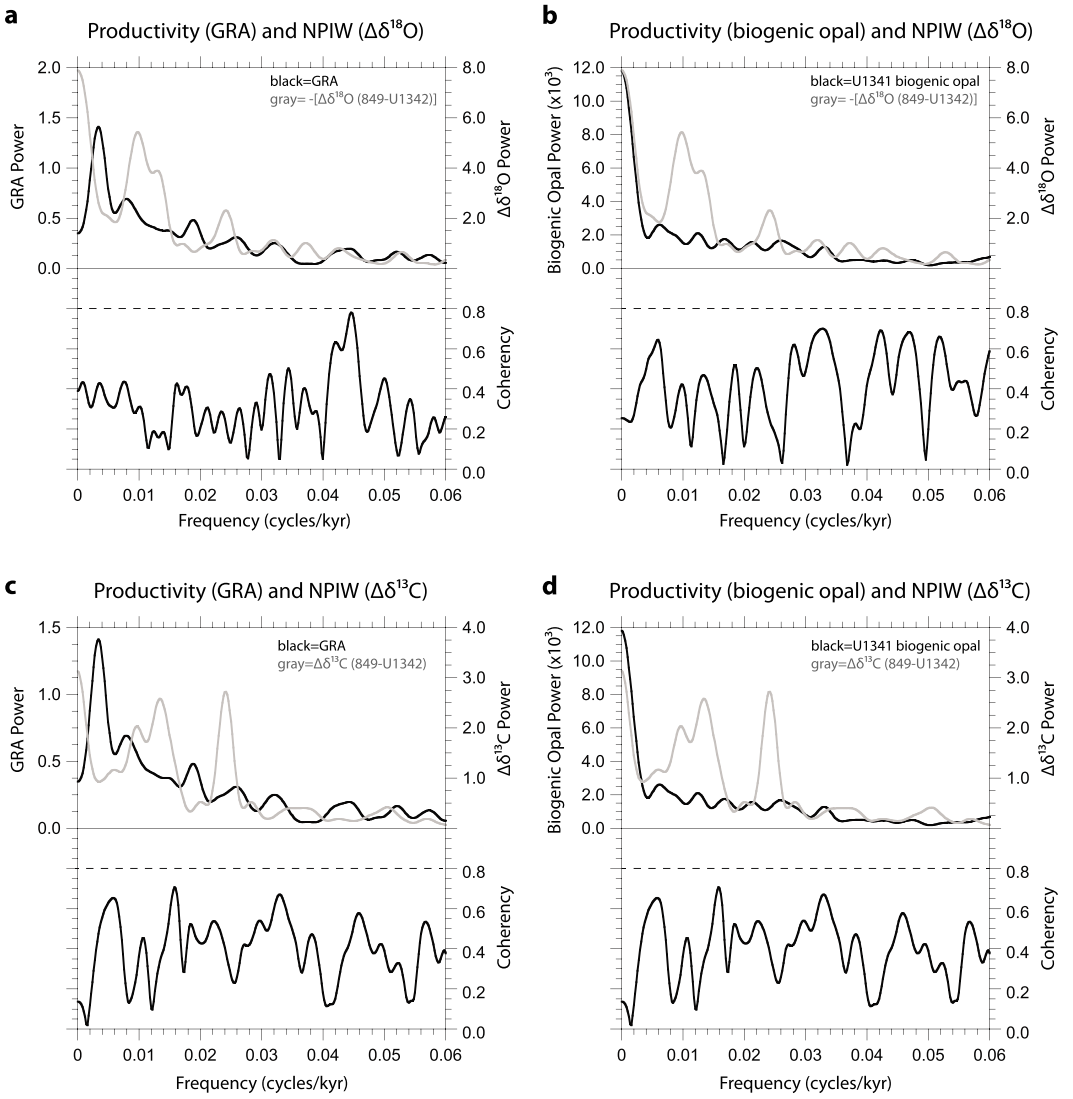

Figure 6. Blackman-Tukey spectral analyses show that primary productivity is independent of NPIW proxies. (a) U1342 gamma ray attenuation (GRA, i.e., density) versus NPIW proxy $\Delta\delta^{18}O_{849\text{-}U1342}$, (b) U1341 biogenic opal versus NPIW proxy $\Delta\delta^{18}O_{849\text{-}U1342}$, (c) U1342 GRA versus NPIW proxy $\Delta\delta^{13}C_{849\text{-}U1342}$, and (d) U1341 biogenic opal [*Asahi et al.*, 2014] versus NPIW proxy $\Delta\delta^{13}C_{849\text{-}U1342}$. Low coherence ($<0.8$, as marked by dotted line in bottom panels) between proxies of primary productivity and NPIW proxies ($\Delta\delta^{13}C$ and $\Delta\delta^{18}O$) demonstrates that these two variables are not strongly correlated at U1342, justifying the use of $\Delta\delta^{13}C$ and $\Delta\delta^{18}O$ as NPIW indicators.

source, and $\Delta\delta^{13}C$ decreases (Figure 4b). As such, we interpret relatively high/low $\Delta\delta^{13}C$ values to indicate reduced/enhanced NPIW at U1342.

The idea that the two proxies, $\Delta\delta^{18}O$ and $\Delta\delta^{13}C$, are both influenced by changes in NPIW ventilation is supported by strong statistical significance between the two variables ($p < 0.0001$). A cross-plot of these two variables (supporting information Figure S2) shows their significant correlation and demonstrates that each time series from U1342 can be used to indicate NPIW prominence. The correlation is not perfect, suggesting that other sources of isotope variability exist. For example, there is apparently millennial-scale variability (Figure 2) that may add "noise" to the data set. We focus here on the orbital G/IG variability; the robustness of our interpretations is reinforced by the mutual agreement of these two NPIW proxies and the length of our records, which allows for the statistical evaluation of many iterations of orbital G/IG cycles (see section 8.1) in order to determine recurring trends.

Table 3. Correlation of U1342 Proxies of Primary Productivity and NPIW

Records Compared	Proxy Interpretation	Pearson Correlation Coefficient (*R*)
Wt % C versus $\Delta\delta^{13}C$ (849-U1342)	Productivity versus NPIW	0.11
CMAR versus $\Delta\delta^{13}C$ (849-U1342)	Productivity versus NPIW	0.24
GRA versus wt % C	Density versus productivity	−0.75
GRA versus CMAR	Density versus productivity	−0.41
GRA versus $\Delta\delta^{13}C$ (849-U1342)[a]	Productivity versus NPIW	−0.15

[a]All records compared are from ~250 ka, except for GRA versus $\Delta\delta^{13}C$ (from 1.2 Ma).

7.2. Validation of the $\Delta\delta^{13}C$ NPIW Proxy

While the validity of using $\Delta\delta^{18}O$ as an indicator of local brine and NPIW was already discussed (see section 6.1), some potential complexity with $\delta^{13}C_c$ interpretations makes it necessary to examine the validity of the use of $\Delta\delta^{13}C$ as an NPIW indicator. Specifically, because productivity is high in the Bering Sea [*Kim et al.*, 2011; *Riethdorf et al.*, 2013; *Schlung et al.*, 2013], it is necessary to establish that *U. peregrina* $\delta^{13}C_c$ is a robust indicator of changes in local bottom water $\delta^{13}C_{DIC}$. Therefore, we performed analyses to rule out the possibility that the record of changes in $\delta^{13}C_c$ of this species is affected by changes in "habitat effects" correlating with the accumulation rate of organic carbon (primary productivity). Changes in habitat effects have been shown in *U. peregrina* from the eastern Atlantic, off the coast of northwest Africa, [*Zahn et al.*, 1986] but have not been extensively studied in low-oxygen environments, such as Site U1342.

Our data demonstrate that $\Delta\delta^{13}C$ values are not correlated with primary productivity (Figures 5 and 6 and Table 3), indicating that the $\delta^{13}C_c$ of *U. peregrina* was not strongly influenced by enhanced carbon flux and respiration in the sediment and thus can be interpreted with confidence as a proxy for the $\delta^{13}C_{DIC}$ of bottom water. Carbonate-free sediments from the past ~250 kyr were analyzed for wt % C and carbon mass accumulation rate (CMAR), two indicators of primary productivity [*Meyers and Teranes*, 2001; *Zahn et al.*, 1986]. There is a weak correlation of $\Delta\delta^{13}C$ with wt % C ($R = 0.11$) and CMAR ($R = 0.24$), as shown in Figure 5. Additionally, laminated sediments indicative of high productivity intervals [*Schlung et al.*, 2013] are not associated with excursions of $\Delta\delta^{13}C$ (Figure 5). From these comparisons, it is evident that the $\Delta\delta^{13}C$ record (and therefore the U1342 $\delta^{13}C_c$ record) is not dominantly influenced by primary productivity over the past ~250 kyr. Additionally, while wt % C and CMAR results are only available for the first ~250 kyr, a strong correlation (Table 3) of these two proxies to density (measured by gamma ray attenuation; GRA) indicates that GRA can be used as a proxy for primary productivity throughout the entire U1342 record.

GRA values show weak correlation to $\Delta\delta^{13}C$ over the 1.2 Myr record ($R = -0.15$; Figure 6c), in agreement with the results from the last ~250 kyr (Figure 5c). Additionally, a long record of biogenic opal%, another proxy for primary productivity, from nearby Site U1341 [*Asahi et al.*, 2014] shows little correlation to our record of $\Delta\delta^{13}C$ (Figure 6d). Together, this multiproxy comparison provides confidence that U1342 *U. peregrina* $\delta^{13}C_c$ is not dominated by the effects of changes in the organic carbon accumulation rates and thus is not heavily influenced by habitat effects. This conclusion, along with the strong correlation between $\Delta\delta^{13}C$ and $\Delta\delta^{18}O$ (a measurement that is not complicated by habitat effects because *U. peregrina* calcifies $\delta^{18}O$ in equilibrium with seawater [*Shackleton*, 1974]), justifies the use of $\delta^{13}C_c$ in calculations of $\Delta\delta^{13}C$ to indicate fluctuations in NPIW.

Additionally, in our study, we are not concerned about the possible effects of air-sea fractionation on the $\delta^{13}C_c$ record. Surface water does not reach the depths of U1342 today [*Warren*, 1983], meaning that the site was likely buffered from the effects of air-sea $\delta^{13}C$ fractionation during interglacials. During glacials, U1342 was affected by NPIW from a local surface water source containing a relatively high $\delta^{13}C_{sw}$ due to both air-sea and photosynthetic fractionation typical of high-latitude surface waters. Our study focuses on the relative (rather than quantitative) changes in NPIW, and air-sea interactions would merely influence the amplitude but not the direction and pattern of the recorded $\delta^{13}C_c$.

8. Changes in NPIW Over the Last 1.2 Myr

8.1. NPIW Relationship to Climate and the Bering Strait

To assess whether the closure of the Bering Strait has an influence on NPIW, we examine the difference between NPIW proxies during glacials and interglacials and use relative sea level (RSL) to distinguish glacials

Table 4. Average and standard deviation of NPIW proxies during open and closed Bering Strait conditions from 1.2 Ma[a]

		All Glacials	G-CBS	G-OBS	All interglacials
$\Delta\delta^{13}$C (849-U1342)	Average	0.164[b]	0.106[c]	0.244	0.244
	SD	0.212	0.162	0.246	0.211
$\Delta\delta^{18}$O (849-U1342)	Average	0.190[b]	0.370[c]	−0.059	0.067
	SD	0.331	0.253	0.256	0.363

[a]See supporting information Table S6 for *t* test results. Glacials with a closed Bering Strait (G-CBS) and glacials with an open Bering Strait (G-OBS) are defined as when relative sea level is below or above the Bering Strait sill depth of 50 m.
[b]Average value is statistically different than interglacial value at $p < 0.01$.
[c]Average value is statistically different than interglacial value at $p < 0.0001$.

with an open Bering Strait (G-OBS) (RSL above −50 m) from glacials with a closed Bering Strait (G-CBS) (RLS below −50 m). G-OBS versus G-CBS conditions yield significantly different results for both mean $\Delta\delta^{18}$O (−0.059‰ versus 0.370‰; $p < 0.0001$) and $\Delta\delta^{13}$C (0.244‰ versus 0.106‰; $p < 0.0001$), which all indicate significantly higher levels of ventilation during G-CBS conditions (Tables 4 and S6). Furthermore, large differences between G-CBS versus interglacial (IG) values of mean $\Delta\delta^{18}$O (0.370‰ versus 0.067‰; $p < 0.0001$) and $\Delta\delta^{13}$C (0.106‰ versus 0.244‰; $p < 0.0001$) show that ventilation was considerably stronger during G-CBS compared to IG conditions, while matching values of mean $\Delta\delta^{13}$C during G-OBS versus IG conditions (0.244‰ versus 0.244‰; $p = 0.987$) show that ventilation was similarly weak whenever the Bering Strait was open, regardless of the climate (Tables 4 and S6). Together, these data indicate that glacial climate alone did not induce more prominent NPIW. Enhanced NPIW in the Bering Sea was only regularly associated with *extreme* glacial conditions, when sea level cut off circulation through the Bering Strait.

Cross-spectral analyses (Figure 7) verify the idea that variations in NPIW are linked to extreme glacial climates when flow through the Bering Strait was cut off. Comparison of NPIW ($\Delta\delta^{13}$C) with the LR04 stack indicates a phase lag whereby maximum glacial conditions precede increases in NPIW by ~4 kyr on 41 kyr cycles (Figure 7a); however, the LR04 record incorporates both temperature and ice volume (sea level) variations, which are not in phase [*Shackleton*, 2000]. To isolate sea level effects on NPIW, we conducted a cross-spectral analysis using a RSL record from *Sosdian and Rosenthal* [2009]. These analyses (Figures 7b and 7c) show that variance in the $\Delta\delta^{18}$O and $\Delta\delta^{13}$C records, which reflects local changes in NPIW formation, is significantly correlated to (coherence ≥ 0.8) and in phase with (or nearly in phase with) RSL variations at periodicities centered at 41 kyr (for $\Delta\delta^{13}$C) and at 41 kyr and 93 kyr (for $\Delta\delta^{18}$O). The general behavior that these results suggest is that as climate cools, it may take a long time for the sea level to drop below the Bering Strait depth; however, once the strait is closed, the ventilation response within the Bering Sea is immediate.

One question that should be addressed is whether other factors associated with extreme glacials (besides the closure of the Bering Strait) could be responsible for the correlation between extreme glacials and enhanced NPIW. Although the relationship between sea level and Bering Strait closure is circumstantial given the available data, modeling results support the idea that the closure of the Bering Strait alone can result in major changes in subsurface circulation. Modeling results from *Hu et al*. [2015] showed that *regardless of the background climate*, changes in freshwater flow through the Bering Strait due its closure had a prominent effect of strengthening AMOC, changing Arctic sea ice patterns and altering the temperature in both the North Atlantic and North Pacific. While this model focused on testing the Atlantic circulation response, results from *Hu et al*. [2015] support the idea that extreme glaciations by themselves (without closing the Bering Strait) do not drive major changes in deep/intermediate circulation. Thus, there is a possible causal relationship between sea level (the closure of the Bering Strait) and enhanced NPIW during extreme glacials.

8.2. Changes in NPIW After the Mid-Pleistocene Transition

The idea of extreme glacials leading to enhanced NPIW is also evident when considering long-term global climate history. The Mid-Pleistocene Transition (MPT; 700–1250 ka) marks a global climatic change from dominant low-amplitude, 40 kyr cycles, to high-amplitude, 100 kyr cycles. Results from U1342 (Table 5) show that after the MPT (0–700 ka), average $\Delta\delta^{18}$O were significantly higher and average $\Delta\delta^{13}$C were significantly lower compared to before the MPT (700–1200 ka), indicating stronger ventilation during the recent interval of relatively extreme glaciations and frequent episodes of Bering Strait closure.

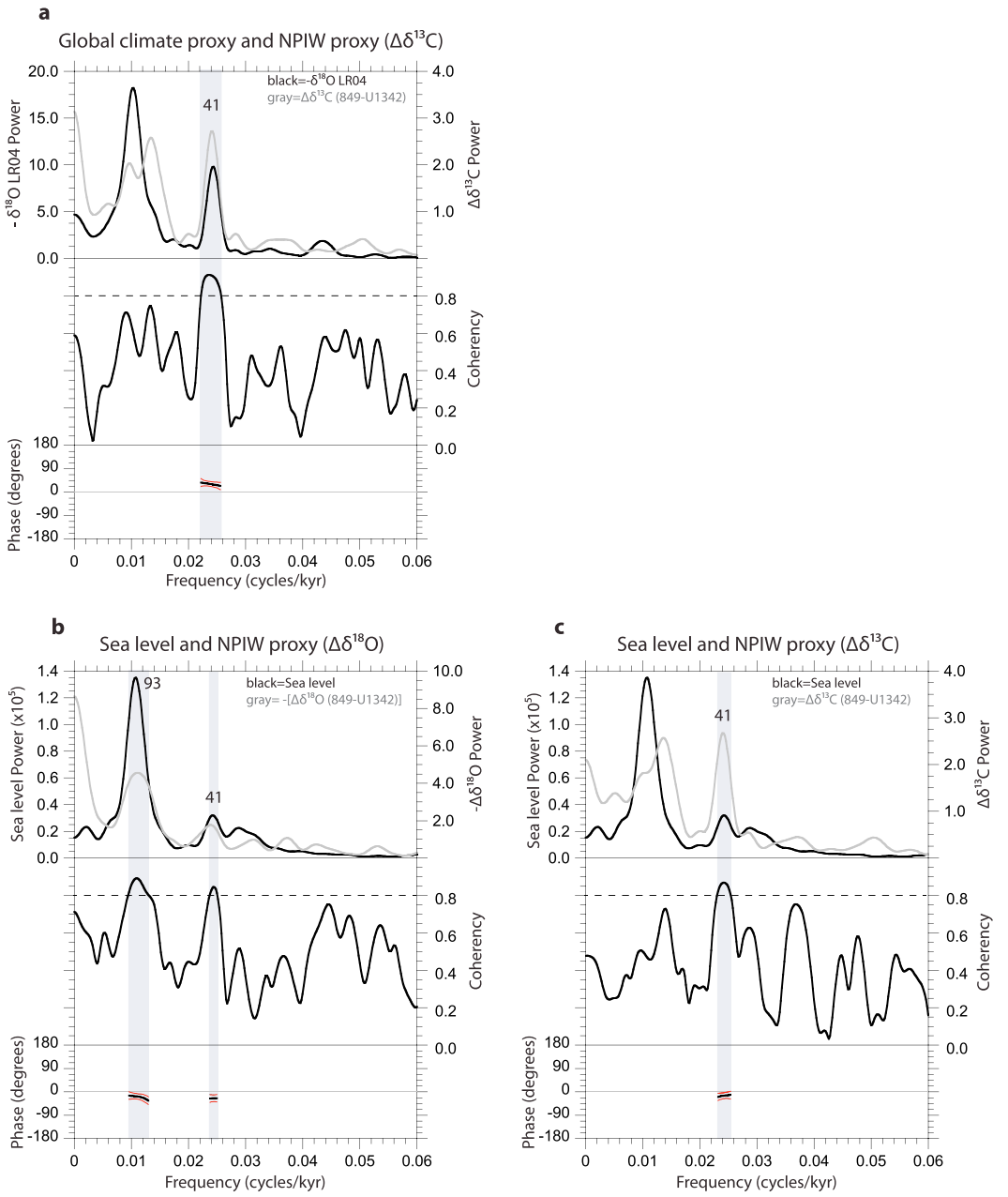

Figure 7. Blackman-Tukey cross-spectral analyses of global climate, sea level, and NPIW. (a) Cross-spectral analysis of $-\delta^{18}O_c$ from the LR04 stack from *Lisiecki and Raymo* [2005], representing a global record of ocean temperature and ice volume, and $\Delta\delta^{13}C_{849\text{-}U1342}$, representing NPIW presence. (b) Relative sea level (RSL) from *Sosdian and Rosenthal* [2009] compared to $-\Delta\delta^{18}O_{849\text{-}U1342}$, a proxy of NPIW production, (c) RSL compared to $\Delta\delta^{13}C_{849\text{-}U1342}$, a proxy of NPIW production. Gray vertical bars highlight frequencies of high coherency (>0.8). Phases (black lines in each bottom panel) were assigned in reference to the first variable in the analysis, and red lines indicate margins of error. Data from Site 849, which was used to calculate proxies of NPIW, is from *Mix et al.* [1995].

8.3. Evaluating the NPIW-NADW Seesaw Hypothesis

New, long NPIW records from U1342 make it possible for the first time to test if the water mass expansion of NPIW and NADW are inversely related to each other, in order to evaluate the seesaw theory proposed by several modeling studies [*Hu et al.*, 2015, 2012a, 2010; *Okazaki et al.*, 2010; *Saenko et al.*, 2004]. AMOC is associated with North Atlantic Deep Water (NADW), which has two components: lower NADW (LNADW; deeper than 2000 m) and upper NADW (UNADW; shallower than 2000 m). North Atlantic sites ODP 982 (57°31′N,

Table 5. Average Benthic Stable Isotope Values Before and After the Mid-Pleistocene Transition[a]

	0–700 ka		700–1200 ka		
	Average (‰)	Standard Deviation	Average (‰)	Standard Deviation	*p* Value
$\delta^{18}O$ (U1342)	3.93	0.22	3.97	0.17	<0.001
$\delta^{13}C$ (U1342)	−0.26	0.18	−0.54	0.19	<0.0001
$\Delta\delta^{18}O$ (849-U1342)	0.21	0.33	0.04	0.27	<0.0001
$\Delta\delta^{13}C$ (849-U1342)	0.14	0.21	0.25	0.21	<0.0001

[a]Data for Site 849 (deep equatorial Pacific) are from *Mix et al.* [1995].

15°53′W; 1135 m) [*Venz et al.*, 1999] and DSDP Site 607 (41°00′N, 32°58′W; 3427 m) [*Ruddiman et al.*, 1989] are ideally located to monitor changes in UNADW and LNADW, respectively. While more comparison sites would be preferable for establishing basin-wide changes in ventilation, there are few North Atlantic records of sufficient length for comparison to Site U1342, so we must rely on these two iconic sites for our evaluation. AMOC strength is difficult to quantify with $\delta^{13}C$ and $\delta^{18}O$ data, but changes in the *relative contribution* of newly formed deep water can be monitored using $\Delta\delta^{13}C$. Thus, to monitor UNADW formation, we use $\delta^{13}C_c$ at ODP Site 982 to calculate $\Delta\delta^{13}C_{849\text{-}982}$ values (Site 849 $\delta^{13}C_c$ − ODP 982 $\delta^{13}C_c$), and to monitor LNADW formation, we use $\delta^{13}C_c$ at DSDP Site 607 to calculate $\Delta\delta^{13}C_{849\text{-}607}$ values (Site 849 $\delta^{13}C_c$ − DSDP 607 $\delta^{13}C_c$). The $\delta^{13}C_c$ records from ODP Site 982 and DSDP Site 607 are shown in the supporting information Figure S3, along with the resulting $\Delta\delta^{13}C$ values. These $\Delta\delta^{13}C$ records of UNADW and LNADW can then be compared to our record of NPIW from U1342 ($\Delta\delta^{13}C_{849\text{-}U1342}$) to determine whether or not there is an antiphase relationship.

Cross-spectral analyses indicate that NPIW and UNADW variability is coherent and in phase, or nearly in phase (NPIW lags UNADW by ~3 kyr), depending on the periodicity (Figures 8a and 8b). However, NPIW and LNADW variability is uncorrelated (Figures 8c and 8d). Therefore, the relative contributions of NPIW in the Bering Sea and UNADW in the North Atlantic appear to increase and decrease simultaneously, and trends in NPIW and LNADW formation are unrelated. It is possible that these results cannot distinguish between the strength of the UNADW/LNADW water mass and a change in its depth. However, if these records were only affected by a change in water mass position and not ventilation strength, we would expect that the records of LNADW and UNADW would be antiphase, which is not the case (supporting information Figure S3). Regardless of these considerations, we can conclude that these results do not demonstrate an antiphase relationship between NPIW and NADW and therefore challenge the NPIW-NADW seesaw theory predicted by models, at least in as much as the theory applies to orbital-scale variations. Because $\delta^{13}C_c$ is not a direct measure of changes in AMOC or PMOC strength, more work is needed to quantify changes in circulation and the mechanisms driving such changes; however, the coherent and in-phase pattern of $\delta^{13}C_c$ variability in NPIW and UNADW provides tentative evidence that the Pacific and Atlantic are linked through a mechanism on orbital timescales that results in in-phase variations in intermediate water circulation, rather than a seesaw.

8.4. Mechanism for NPIW During Extreme Glacials

Our $\delta^{18}O$ results (section 6) indicate that brine rejection from enhanced sea ice formation within the Bering Sea is critically important to NPIW formation during extreme glacials of the past 1.2 Myr, and we suggest that Bering Sea brine formation is key to explaining why our data show in-phase NPIW-UNADW coupling while models predict seesaw behavior. Although models include dynamic sea ice processes and convective/open ocean NPIW formation, they do not have high enough resolution to simulate sea ice formation on continental shelves, where brine formation is most critical. Because NPIW formation via brine rejection on shelves is not well represented in current Bering Strait closure models, models may predict weak (rather than strong) NPIW formation during Bering Strait closure.

While the results of this study indicate that Bering Sea brine formation was enhanced when the Bering Strait was closed, the reason for this relationship is less clear. The exact mechanism for the brine formation is outside the scope of our data, but models can offer important insight into parameters (e.g., temperature and atmospheric patterns) that could create conditions amenable for brine formation, even if the models do not adequately simulate brine formation itself. We suggest that one mechanism invoking brine that possibly explains why NPIW is enhanced during glacials, and thus why our data show that NPIW and UNADW

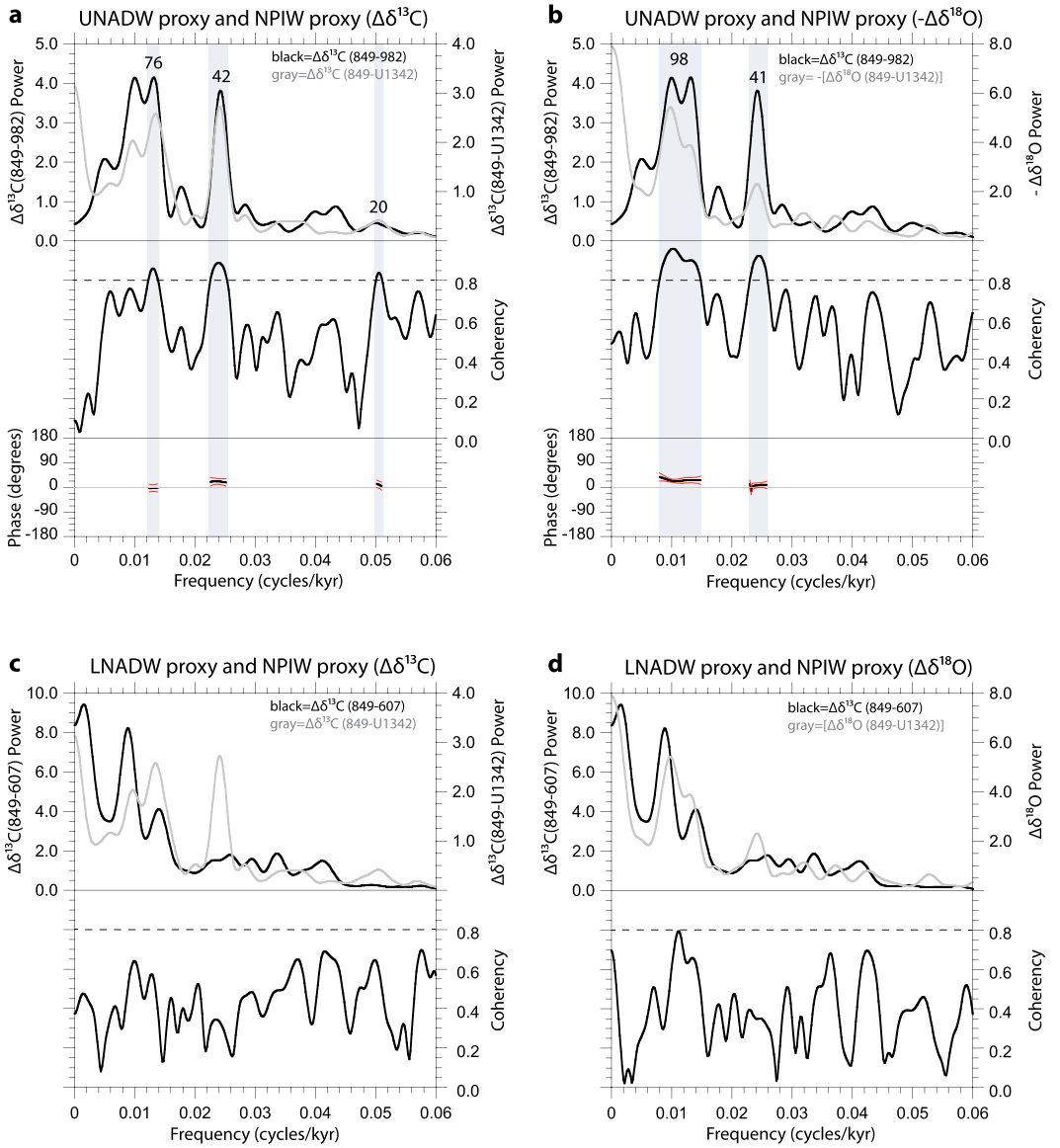

Figure 8. Blackman-Tukey cross-spectral analyses of UNADW and LNADW versus NPIW do not support an orbital-scale NPIW-NADW seesaw. (a) UNADW proxy $\Delta\delta^{13}C_{849\text{-}982}$ versus NPIW proxy $\Delta\delta^{13}C_{849\text{-}U1342}$, (b) UNADW proxy versus NPIW proxy $\Delta\delta^{18}O_{849\text{-}U1342}$, (c) LNADW proxy $\Delta\delta^{13}C_{849\text{-}607}$ versus NPIW proxy $\Delta\delta^{13}C_{849\text{-}U1342}$, and (d) LNADW proxy versus NPIW proxy $\Delta\delta^{18}O_{849\text{-}U1342}$. Gray vertical bars indicate frequencies of high coherency (>0.8; dotted black line), which show that UNADW is in phase, or nearly in phase, with NPIW (Figures 8a and 8b), whereas LNADW and NPIW are weakly correlated (Figures 8c and 8d). Phase (black line in bottom panel) was assigned in reference to UNADW and LNADW, and red lines indicate margins of error. $\delta^{13}C_c$ data used to calculate NPIW, UNADW, and LNADW were from the following sources: *Mix et al.* [1995] (Site 849; 3839 m), *Venz et al.* [1999] (Site 982; 1145 m), and *Ruddiman et al.* [1989] (Site 607; 3427 m).

formation are nearly in phase, involves the impact of the Bering Strait closure on Bering Sea temperature and sea ice formation. When Bering Strait closure cuts off the freshwater input to the North Atlantic, models show that this results in increased salinity, enhanced UNADW formation, and warming [*Hu et al.*, 2012a]. Concurrently, the modeled seesaw behavior arises from the fact that models predict that closing the Bering Strait and isolating freshwater within the North Pacific results in less saline and colder sea surface temperatures [*Hu et al.*, 2015, 2010], and hence, deep convection and NPIW formation in the models is inhibited. Since our data show that NPIW is actually enhanced, there must be a mechanism, which is poorly represented in models, by which colder and less saline sea surface conditions in the Bering Sea promote, rather than inhibit, NPIW formation.

It is possible that the cooler temperatures during intervals of Bering Strait closure were accompanied by major changes in atmospheric conditions that could have enhanced sea ice formation and NPIW via brine formation on/near shelves even while open ocean convection was inhibited. In the modern climate system, very cold North Pacific winters are associated with an easterly shift in the Aleutian Low [*Luchin et al.*, 2002; *Rodionov et al.*, 2007]. This shift may result in more northerly winds over the Bering Sea, moving sea ice southward and extending the polynya growth regions [*Rodionov et al.*, 2007]. Therefore, we propose that an easterly shift in the Aleutian Low during extreme glacials could have enhanced Bering Sea polynya growth, resulting in strong brine rejection; thus, although the North Pacific/Bering Sea surface water may have been fresher on a regional scale, glacial NPIW production would have been promoted in *localized* areas (polynyas) within the Bering Sea (as it is today within Okhotsk Sea polynyas). This mechanism, which is partially supported by model results that suggest opening/closing the Bering Strait can directly affect the Aleutian Low [*Okumura et al.*, 2009], would most easily explain the increase in Bering Sea brine production, since wind direction is the primary control on sea ice extent within the Bering Sea [*Overland and Pease*, 1982].

9. Conclusions

New records of foraminiferal $\delta^{18}O$ and $\delta^{13}C$ from Bering Sea Site U1342 provide an unparalleled opportunity to investigate past changes in Bering Sea climate and ocean circulation since 1.2 Ma. This study provides the first evidence of recurring NPIW ventilation during extreme glacial climates over multiple G/IG cycles and also demonstrates that NPIW ventilation was caused by local sea brine formation within the Bering Sea. Due to the unprecedented length and detail of our Bering Sea record, we were able to conduct robust statistical analyses of the orbital-scale variability, which revealed that enhanced NPIW ventilation occurred only during extreme glacial events, in which the Bering Strait was closed (sea level dropped at least 50 m relative to present). Finally, our long records of NPIW provide the first opportunity to evaluate the NPIW-NADW seesaw hypothesis using paleoceanographic data. Our results show evidence that NPIW was enhanced simultaneously with UNADW on orbital timescales, and NPIW had no relationship to LNADW. These results, which do not demonstrate an orbital-scale antiphase relationship between NPIW and NADW, provide preliminary evidence contradicting seesaw behavior predicted by many models. We suggest that NPIW formation via brine formation on and near continental shelves, which is not adequately simulated in models, may explain data-model discrepancies.

Accurately discerning the behavior of NPIW in relation to NADW is essential to understanding MOC, oceanic heat transfer, and global climate. The effects of closing the Bering Strait are thought to be profound based on modeling results, but these models need to be ground truthed by paleoceanographic data. Some climate models show that the closure of the Bering Strait may result in a ~15% decrease of meridional heat transport, and thus ~1.5°C cooling in the North Pacific [*Hu et al.*, 2015, 2010] (relative to an open Bering Strait scenario), while others show the opposite response [*Okumura et al.*, 2009]. Additionally, AMOC-PMOC seesaw behavior has been shown to result in buffered Northern Hemisphere cooling during intervals of AMOC shutdown [*Okazaki et al.*, 2010] and is used to explain extreme climatic events of the last deglaciation [*De Boer and Nof*, 2004; *Hu et al.*, 2012a, 2012b]. Our U1342 records validate the idea of a robust relationship between NPIW prominence and flow through the Bering Strait but also provide orbital-scale evidence that contradicts modeling studies that demonstrate an NPIW-NADW seesaw with Bering Strait closure. Thus, substantial work is needed both to confirm our data-based results and to understand the source of model-data mismatches. Accurately discerning changes in NPIW and NADW will have significant implications for our understanding of the climate system.

Acknowledgments
This research used samples and data from the Integrated Ocean Drilling Program (IODP). Funding for this research was provided by a Schlanger Ocean Drilling Fellowship from the Consortium for Ocean Leadership and NSF grant OCE0963144. We would like to thank Dyke Andreasen for his help with instrumentation, as well as Ivano Aiello, Mea Cook, Aixue Hu, Axel Timmermann, James Zachos, and anonymous reviewers for their helpful discussions and comments on our manuscript. We also thank several members of the Ravelo Lab for laboratory assistance. K.P. Knudson conducted the analytical and statistical analyses and wrote the paper with the guidance of A.C. Ravelo. We declare no competing financial interests.

References

Asahi, H., S. Kender, M. Ikehara, T. Sakamoto, K. Takahashi, A. C. Ravelo, C. A. Alvarez Zarikian, B. K. Khim, and M. J. Leng (2014), Orbital-scale benthic foraminiferal oxygen isotope stratigraphy at the northern Bering Sea Slope Site U1343 (IODP Expedition 323) and its Pleistocene paleoceanographic significance, *Deep Sea Res., Part II*, doi:10.1016/j.dsr2.2014.01.004.

Boyle, E. A., and L. D. Keigwin (1985), Comparison of Atlantic and Pacific paleochemical records for the last 215,000 years: Changes in deep ocean circulation and chemical inventories, *Earth Planet. Sci. Lett.*, *76*, 135–150.

Brennan, C. E., K. J. Meissner, M. Eby, C. Hillaire-Marcel, and A. J. Weaver (2013), Impact of sea ice variability on the oxygen isotope content of seawater under glacial and interglacial conditions, *Paleoceanography*, *28*, 388–400, doi:10.1002/palo.20036.

Bryan, S. P., and T. M. Marchitto (2008), Mg/Ca-temperature proxy in benthic foraminifera: New calibrations from the Florida Straits and a hypothesis regarding Mg/Li, *Paleoceanography*, *23*, PA2220, doi:10.1029/2007PA001553.

Clark, P. U., J. X. Mitrovica, G. A. Milne, and M. E. Tamisiea (2002), Sea-level fingerprinting as a direct test for the source of global meltwater pulse IA, *Science*, *295*(5564), 2438–2441.
Cook, M. S., L. D. Keigwin, and C. A. Sancetta (2005), The deglacial history of surface and intermediate water of the Bering Sea, *Deep Sea Res., Part II*, *52*(16–18), 2163–2173.
Curry, W. B., and D. W. Oppo (2005), Glacial water mass geometry and the distribution of $\delta^{13}C$ of Sigma CO_2 in the western Atlantic Ocean, *Paleoceanography*, *20*, PA1017, doi:10.1029/2004PA001021.
De Boer, A. M., and D. Nof (2004), The Bering Strait's grip on the Northern Hemisphere climate, *Deep Sea Res., Part I*, *51*(10), 1347–1366.
Duplessy, J. C., N. J. Shackleton, R. K. Matthews, W. Prell, W. F. Ruddiman, M. Caralp, and C. H. Hendy (1984), $\delta^{13}C$ record of benthic foraminifera in the last interglacial ocean: Implications for the carbon cycle and the global deep water circulation, *Quat. Res.*, *21*(2), 225–243.
Expedition 323 Scientists (2010), Bering Sea paleoceanography: Pliocene–Pleistocene paleoceanography and climate history of the Bering Sea, *IODP Prel. Rept.*, *323*, doi:10.2204/iodp.pr.323.2010.
Expedition 323 Scientists (2011), Site U1342, in *Proceedings of the Integrated Ocean Drilling Program*, vol. 323, edited by K. Takahashi et al., pp. 1–71, Integrated Ocean Drill. Program Manage. Int., Inc., Tokyo, doi:10.2204/iodp.proc.323.106.2011.
Gebhardt, H., M. Sarnthein, P. M. Grootes, T. Kiefer, H. Kuehn, F. Schmieder, and U. Rohl (2008), Paleonutrient and productivity records from the subarctic North Pacific for Pleistocene glacial terminations I to V, *Paleoceanography*, *23*, PA4212, doi:10.1029/2007PA001513.
Herguera, J. C., E. Jansen, and W. H. Berger (1992), Evidence for a bathyal front at 2000 m depth in the glacial Pacific, based on a depth transect on the Ontong Java Plateau, *Paleoceanography*, *7*(3), 273–288, doi:10.1029/92PA00869.
Hillaire-Marcel, C., and A. de Vernal (2008), Stable isotope clue to episodic sea ice formation in the glacial North Atlantic, *Earth Planet. Sci. Lett.*, *268*(1–2), 143–150.
Horikawa, K., Y. Asahara, K. Yamamoto, and Y. Okazaki (2010), Intermediate water formation in the Bering Sea during glacial periods: Evidence from neodymium isotope ratios, *Geology*, *38*(5), 435–438.
Hu, A. X., G. A. Meehl, B. L. Otto-Bliesner, C. Waelbroeck, W. Q. Han, M. F. Loutre, K. Lambeck, J. X. Mitrovica, and N. Rosenbloom (2010), Influence of Bering Strait flow and North Atlantic circulation on glacial sea-level changes, *Nat. Geosci.*, *3*(2), 118–121.
Hu, A. X., G. A. Meehl, W. Q. Han, A. Abe-Ouchi, C. Morrill, Y. Okazaki, and M. O. Chikamoto (2012a), The Pacific-Atlantic seesaw and the Bering Strait, *Geophys. Res. Lett.*, *39*, L03702, doi:10.1029/2011GL050567.
Hu, A. X., et al. (2012b), Role of the Bering Strait on the hysteresis of the ocean conveyor belt circulation and glacial climate stability, *Proc. Natl. Acad. Sci. U.S.A.*, *109*(17), 6417–6422.
Hu, A. X., G. A. Meehl, W. Q. Han, B. Otto-Bliestner, A. Abe-Ouchi, and N. Rosenbloom (2015), Effects of the Bering Strait closure on AMOC and global climate under different background climates, *Prog. Oceanogr.*, *132*, 174–196.
Jaccard, S. L., and E. D. Galbraith (2013), Direct ventilation of the North Pacific did not reach the deep ocean during the last deglaciation, *Geophys. Res. Lett.*, *40*, 199–203, doi:10.1029/2012GL054118.
Lea, D. W., and E. A. Boyle (1993), Determination of carbonate-bound barium in foraminifera and corals by isotope dilution plasma-mass spectrometry, *Chem. Geol.*, *103*, 73–84.
Kallel, N., L. D. Labeyrie, A. Juilletleclerc, and J. C. Duplessy (1988), A deep hydrological front between intermediate and deep water masses in the glacial Indian Ocean, *Nature*, *333*(6174), 651–655.
Keigwin, L. D. (2004), Radiocarbon and stable isotope constraints on Last Glacial Maximum and Younger Dryas ventilation in the western North Atlantic, *Paleoceanography*, *19*, PA4012, doi:10.1029/2004PA001029.
Kim, S., B. K. Khim, M. Uchida, T. Itaki, and R. Tada (2011), Millennial-scale paleoceanographic events and implication for the intermediate-water ventilation in the northern slope area of the Bering Sea during the last 71 kyrs, *Global Planet. Change*, *79*(1–2), 89–98.
LeGrande, A. N., and G. A. Schmidt (2006), Global gridded data set of the oxygen isotopic composition in seawater, *Geophys. Res. Lett.*, *33*, L12604, doi:10.1029/2006GL026011.
Lisiecki, L. E. (2010), A simple mixing explanation for late Pleistocene changes in the Pacific-South Atlantic benthic $\delta^{13}C$ gradient, *Clim. Past*, *6*(3), 305–314.
Lisiecki, L. E., and M. E. Raymo (2005), A Pliocene-Pleistocene stack of 57 globally distributed benthic $\delta^{18}O$ records, *Paleoceanography*, *20*, PA1003, doi:10.1029/2004PA001071.
Luchin, V. A., I. P. Semiletov, and G. E. Weller (2002), Changes in the Bering Sea region: Atmosphere-ice-water system in the second half of the twentieth century, *Prog. Oceanogr.*, *55*(1–2), 23–44.
Matsumoto, K., T. Oba, J. Lynch-Stieglitz, and H. Yamamoto (2002), Interior hydrography and circulation of the glacial Pacific Ocean, *Quat. Sci. Rev.*, *21*(14–15), 1693–1704.
Max, L., J. R. Riethdorf, R. Tiedemann, M. Smirnova, L. Lembke-Jene, K. Fahl, D. Nurnberg, A. Matul, and G. Mollenhauer (2012), Sea surface temperature variability and sea-ice extent in the subarctic northwest Pacific during the past 15,000 years, *Paleoceanography*, *27*, PA3213, doi:10.1029/2012PA002292.
Max, L., L. Lembke-Jene, J. R. Riethdorf, R. Tiedemann, D. Nurnberg, H. Kuhn, and A. Mackensen (2014), Pulses of enhanced North Pacific Intermediate Water ventilation from the Okhotsk Sea and Bering Sea during the last deglaciation, *Clim. Past*, *10*(2), 591–605.
Menviel, L., A. Timmermann, O. Elison Timm, A. Mouchet, A. Abe-Ouchi, M. O. Chikamoto, N. Harada, R. Ohgaito, and Y. Okazaki (2012), Removing the North Pacific halocline: Effects on global climate, ocean circulation and the carbon cycle, *Deep Sea Res., Part II*, *61–64*, 106–113.
Meyers, P. A., and J. L. Teranes (2001), Sediment organic matter, in *Tracking Environmental Change Using Lake Sediments*, edited by W. M. Last and J. P. Smol, pp. 239–269, Springer, Netherlands.
Mix, A. C., N. G. Pisias, W. Rugh, J. Wilson, A. Morey, and T. K. Hagelberg (1995), Benthic foraminifer stable isotope record from Site 849 (0–5 Ma): Local and global climate changes, in *Proceedings of the Ocean Drilling Program, Sci. Res.*, vol. 138, edited by N. G. Pisias et al., pp. 371–412, Ocean Drill. Program, College Station, Tex.
Ohkushi, K., T. Itaki, and N. Nemoto (2003), Last Glacial-Holocene change in intermediate-water ventilation in the northwestern Pacific, *Quat. Sci. Rev.*, *22*(14), 1477–1484.
Okazaki, Y., K. Takahashi, H. Asahi, K. Katsuki, J. Hori, H. Yasuda, Y. Sagawa, and H. Tokuyama (2005), Productivity changes in the Bering Sea during the late Quaternary, *Deep Sea Res., Part II*, *52*(16–18), 2150–2162.
Okazaki, Y., A. Timmermann, L. Menviel, N. Harada, A. Abe-Ouchi, M. O. Chikamoto, A. Mouchet, and H. Asahi (2010), Deepwater formation in the North Pacific during the Last Glacial Termination, *Science*, *329*(5988), 200–204.
Okumura, Y. M., C. Deser, A. Hu, A. Timmermann, and S. P. Xie (2009), North Pacific climate response to freshwater forcing in the subarctic North Atlantic: Oceanic and atmospheric pathways, *J. Clim.*, *22*(6), 1424–1445.
Overland, J. E., and C. H. Pease (1982), Cyclone climatology of the Bering Sea and its relation to sea ice extent, *Mon. Weather Rev.*, *110*(1), 5–13.

Paillard, D. L., L. Labeyrie, and P. Yiou (1996), Machintosh program performs time-series analysis, *Eos Trans. AGU*, *77*(39), 379–379, doi:10.1029/96EO00259.
Ravelo, A. C., and C. Hillaire-Marcel (2007), The use of oxygen and carbon isotopes of foraminifera in studies of paleoceanography, in *Proxies in Late Cenozoice Paleoceanography, Developments in Marine Geology*, edited by C. Hillaire-Marcel and A. de Vernal, Elsevier, Amsterdam.
Rella, S. F., R. Tada, K. Nagashima, M. Ikehara, T. Itaki, K. Ohkushi, T. Sakamoto, N. Harada, and M. Uchida (2012), Abrupt changes of intermediate water properties on the northeastern slope of the Bering Sea during the last glacial and deglacial period, *Paleoceanography*, *27*, PA3203, doi:10.1029/2011PA002205.
Riethdorf, J. R., D. Nurnberg, L. Max, R. Tiedemann, S. A. Gorbarenko, and M. I. Malakhov (2013), Millennial-scale variability of marine productivity and terrigenous matter supply in the western Bering Sea over the past 180 kyr, *Clim. Past*, *9*(3), 1345–1373.
Rodionov, S. N., N. A. Bond, and J. E. Overland (2007), The Aleutian Low, storm tracks, and winter climate variability in the Bering Sea, *Deep Sea Res., Part II*, *54*(23–26), 2560–2577.
Rohling, E. J., K. Grant, M. Bolshaw, A. P. Roberts, M. Siddall, C. Hemleben, and M. Kucera (2009), Antarctic temperature and global sea level closely coupled over the past five glacial cycles, *Nat. Geosci.*, *2*(7), 500–504.
Ruddiman, W. F., M. E. Raymo, D. G. Martinson, B. M. Clement, and J. Backman (1989), Pleistocene evolution: Northern Hemisphere ice sheets and North Atlantic Ocean, *Paleoceanography*, *4*(4), 353–412, doi:10.1029/PA004i004p00353.
Saenko, O. A., A. Schmittner, and A. J. Weaver (2004), The Atlantic-Pacific seesaw, *J. Clim.*, *17*(11), 2033–2038.
Sarnthein, M., B. Schneider, and P. M. Grootes (2013), Peak glacial ^{14}C ventilation ages suggest major draw-down of carbon into the abyssal ocean, *Clim. Past*, *9*(6), 2595–2614.
Schlung, S. A., et al. (2013), Millennial-scale climate change and intermediate water circulation in the Bering Sea from 90 ka: A high-resolution record from IODP Site U1340, *Paleoceanography*, *28*, 54–67, doi:10.1029/2012PA002365.
Schumacher, J. D., K. Aagaard, C. H. Pease, and R. B. Tripp (1983), Effects of a shelf polynya on flow and water properties in the northern Bering Sea, *J. Geophys. Res.*, *88*(NC5), 2723–2732, doi:10.1029/JC088iC05p02723.
Shackleton, N. J. (1974), Attainment of isotopic equilibrium between ocean water and benthonic foraminifera genus *Uvigerina*: Isotopic changes in the ocean during the last glacial, *Colloq. Int. C. N. R. S.*, *219*, 203–209.
Shackleton, N. J. (2000), The 100,000-year ice-age cycle identified and found to lag temperature, carbon dioxide, and orbital eccentricity, *Science*, *289*(5486), 1897–1902.
Shaffer, G., and J. Bendtsen (1994), Role of the Bering Strait in controlling North Atlantic ocean circulation and climate, *Nature*, *367*(6461), 354–357.
Shcherbina, A. Y., L. D. Talley, and D. L. Rudnick (2003), Direct observations of North Pacific ventilation: Brine rejection in the Okhotsk Sea, *Science*, *302*(5652), 1952–1955.
Sosdian, S., and Y. Rosenthal (2009), Deep-sea temperature and ice volume changes across the Pliocene-Pleistocene climate transitions, *Science*, *325*(5938), 306–310.
Talley, L. D. (2003), Shallow, intermediate, and deep overturning components of the global heat budget, *J. Phys. Oceanogr.*, *33*(3), 530–560.
Tan, F. C., and P. M. Strain (1996), Sea ice and oxygen isotopes in Foxe Basin, Hudson Bay, and Hudson Strait, Canada, *J. Geophys. Res.*, *101*(C9), 20,869–20,876, doi:10.1029/96JC01557.
Tan, F. C., and W. D. Fraser (1976), Oxygen isotope studies on sea ice in Gulf of St. Lawrence, *J. Fish. Res. Board Can.*, *33*(6), 1397–1401.
Tanaka, S., and K. Takahashi (2005), Late Quaternary paleoceanographic changes in the Bering Sea and the western subarctic Pacific based on radiolarian assemblages, *Deep Sea Res., Part II*, *52*(16–18), 2131–2149.
Venz, K. A., D. A. Hodell, C. Stanton, and D. A. Warnke (1999), A 1.0 Myr record of glacial North Atlantic Intermediate Water variability from ODP site 982 in the northeast Atlantic, *Paleoceanography*, *14*(1), 42–52, doi:10.1029/1998PA900013.
Warner, M. J., and G. I. Roden (1995), Chlorofluorocarbon evidence for recent ventilation of the deep Bering Sea, *Nature*, *373*(6513), 409–412.
Warren, B. A. (1983), Why is no deep water formed in the North Pacific?, *J. Mar. Res.*, *41*(2), 327–347.
Woodgate, R. A., T. J. Weingartner, and R. Lindsay (2012), Observed increases in Bering Strait oceanic fluxes from the Pacific to the Arctic from 2001 to 2011 and their impacts on the Arctic Ocean water column, *Geophys. Res. Lett.*, *39*, L24603, doi:10.1029/2012GL054092.
Yasuda, I. (1997), The origin of the North Pacific Intermediate Water, *J. Geophys. Res.*, *102*(C1), 893–909, doi:10.1029/96JC02938.
Zahn, R., K. Winn, and M. Samthein (1986), Benthic foraminiferal δ^{13}C and accumulation rates of organic carbon: *Uvigerina peregrina* group and *Cibicidoides wuellerstorfi*, *Paleoceanography*, *1*(1), 27–42, doi:10.1029/PA001i001p00027.

Erratum

In the originally published version of this article, symbols were missing from variables in Table 4. The table has since been replaced and this version may be considered the authoritative version of record.